Behavioural responses to a photovoltaic subretinal prosthesis implanted in non-human primates

Paul-Henri Prévot, Kevin Gehere, Fabrice Arcizet, Himanshu Akolkar, Mina A Khoei, Kévin Blaize, Omar Oubari, Pierre Daye, Marion Lanoë, Manon Valet, et al.

HAL Id: hal-02505613

https://hal.sorbonne-universite.fr/hal-02505613v1

Submitted on 11 Mar 2020

Behavioural responses to a photovoltaic subretinal prosthesis implanted in non-human primates

Paul-Henri Prévot[1], Kevin Gehere[1], Fabrice Arcizet[1], Himanshu Akolkar[1], Mina A. Khoei[1], Kévin Blaize[1], Omar Oubari[1], Pierre Daye[1], Marion Lanoë[1], Manon Valet[1], Sami Dalouz[1], Paul Langlois[1], Elric Esposito[1], Valérie Forster[1], Elisabeth Dubus[1], Nicolas Wattiez[4], Elena Brazhnikova[1], Céline Nouvel-Jaillard[1], Yannick LeMer[2], Joanna Demilly[3], Claire-Maëlle Fovet[3], Philippe Hantraye[3], Morgane Weissenburger[4], Henri Lorach[5], Elodie Bouillet[6], Martin Deterre[6], Ralf Hornig[6], Guillaume Buc[6], José-Alain Sahel[1,2,7,8], Guillaume Chenegros[1], Pierre Pouget[4&], Ryad Benosman[1,7&], Serge Picaud[1*&]

[1] Sorbonne Université, INSERM, CNRS, Institut de la Vision, 75012 Paris, France
[2] Fondation Ophtalmologique A. de Rothschild, 25-29 rue Manin, 75019 Paris
[3] Molecular Imaging Research Center (MIRCen), 18 route du Panorama, 92265 Fontenay-aux-Roses
[4] Institut du Cerveau et de la Moelle épinière - CNRS UMR 7225 Hôpital de la Pitié-Salpêtrière - 47, bd de l'Hôpital 75646 Paris CEDEX 13
[5] Hansen Experimental Physics Laboratory, Stanford University, Stanford, CA, 94305, USA
[6] Pixium Vision, 74 rue du Faubourg Saint-Antoine, 75012, Paris
[7] Department of Ophthalmology, The University of Pittsburgh School of Medicine, Pittsburgh, PA 15213, United States
[8] CHNO des Quinze-Vingts, DHU Sight Restore, INSERM-DGOS CIC 1423, Paris, France;

[&] These authors contributed equally
* Corresponding author, serge.picaud@inserm.fr

Retinal dystrophies and age-related macular degeneration related to photoreceptor degeneration can cause blindness. In blind patients, although the electrical activation of the residual retinal circuit can provide useful artificial visual perception, the resolutions of current retinal prostheses have been limited either by large electrodes or small numbers of pixels. Here, we report the evaluation, in three awake non-human primates, of a previously reported near-infrared-light-sensitive photovoltaic subretinal prosthesis. We show that multi-pixel stimulation of the prosthesis within radiation-safety limits enabled eye tracking in the animals, that they responded to the stimulations in the direction of the implant with repeated saccades, and that the implant-induced responses were present two years after device implantation. Our findings pave the way for the clinical evaluation of a 378-electrode prosthesis in patients affected by dry atrophic age-related macular degeneration.

One-sentence editorial summary (to appear right below the article's title on the journal's website):
A near-infrared-light-sensitive photovoltaic subretinal prosthesis triggers behavioural responses in awake macaques, even two years after device implantation.

Recent clinical trials have shown that retinal prostheses can restore some visual perception through electrical stimulation of the remaining inner neurons in the degenerated retina[1]. Psychophysics studies in sighted subjects have shown that 600 pixels or distinct percepts are required to restore autonomous locomotion, face recognition and text reading even in a slightly eccentric position[2–6]. A more recent study indicates that, in pessimistic static conditions, 3,000 to 5,000 pixels are likely needed to identify objects within a complex background setting, even using confocal images[7]. Accordingly, successive retinal prosthesis designs have attempted to augment spatial resolution by increasing the number of pixels, from 60 to 1600 pixels[8,9]. However, visual perception with such implanted devices has yet to attain the expected visual acuity. An absence of distinct individual percepts for neighboring electrodes is likely explanation for this. In all such retinal prostheses, electrical currents generated at stimulating electrodes must return to a distant ground. Modeling studies have suggested that this distant ground configuration results in poor confinement of the electrical field. A ground grid that surrounded each stimulating electrode, however, would greatly improve the resolution and contrast of pattern stimulations[10,11]. Using such an architecture, a photovoltaic near-infrared (NIR) sensitive device has been shown to yield high spatial resolutions in rodents[12]. In such a device, each electrode is independently powered by two NIR sensitive photodiodes connected in series between the central electrode and the surrounding hexagonal ground grid (Fig. 1a, see inset). NIR light is planned to be delivered through the patient's pupil via video equipped goggles to stimulate a wireless, modular implant *in vivo*, permitting a less invasive surgical procedure while leveraging object scanning by eye movement. We report here our experience with these ground grid configuration photovoltaic sub-retinal implants *in vitro* and *in vivo* in a primate model. We reliably elicited action potentials in retinal neurons by stimulating single units of the implant *in vitro*, and obtained behavioral responses in prosthesis-implanted primates when stimulated *in vivo*.

In vitro study of the implant in retinal tissue cultures

We adapted the fabrication process of the implants to obtain a clinical-grade device (1.5 mm wide, 30 µm thick, 140 µm electrode pitch, Fig. 1a), and replaced the through holes surrounding each individual pixel that can potentially increase the diffusion of metabolites and oxygen, by solid isolation trenches. We first investigated the efficacy and spatiotemporal resolution of these implants in an *ex vivo* model of a degenerated non-human primate (NHP) retina. We created a blind retina model by sectioning the retina using a vibratome[13], at a thickness that eliminated the photoreceptor layers (Fig. 1b,c). Although this model cannot account for retinal remodeling and inflammation typical of photoreceptor degenerative disease[14], the photoreceptors had to be removed because otherwise they define the membrane potential of ON and OFF bipolar cells in opposite directions. In photoreceptor degenerative diseases, the ON and OFF bipolar neurons are free to set their resting potentials in the absence of photoreceptor glutamate input. The blind NHP retina sections were cultured for 24 to 48 h and recorded with a multi-electrode array (MEA, Fig. 1d). A photovoltaic implant was positioned on the bipolar cell side in place of the removed photoreceptors (Fig. 1e,f), and retinal ganglion cell (RGC) activity (the retinal output) was recorded during stimulation. We varied the intensity and the duration of stimulation pulses of full-field NIR light (880 nm), and measured the threshold values necessary for generating RGC responses. We counted the number of spikes occurring in a 40 ms window that began after the withdrawal of the stimulation artifact (gray rectangle). We observed that the RGCs generated spikes at a low NIR irradiance (0.48 mW mm^{-2}, 2 retinas, 166 cells) for 4 ms flashes (Fig. 1g). No responses were recorded in the NHP blind retina when NIR stimulations were applied beyond the implant. Flash duration was varied from 1 to 10 ms, and we found that peak responses were reached at 7 ms, using full field stimulations at 1 mW mm^{-2} (2 retinas, 166 cells, Fig. 1h). The shortest stimulus resulted in bursts of spikes with latencies greater than 10 ms after the beginning of the stimulation (3.5 mW mm^{-2}, 4 retinas, 99 cells). Latency was estimated at the shortest stimulation duration (1 ms) because the observation of fast responses could be hindered by artifact during longer stimulations. Relatively long latency burst responses are consistent with an indirect activation of RGC requiring bipolar cell stimulation[15–18]. To affirm this hypothesis, synaptic blockers (LAP-4, CPP, CNQX) were introduced into the culture medium during the stimulation. This blockade abolished RGC responses to NIR stimulation, which indicates that their spiking activity was due to bipolar cell activation rather than direct RGC stimulation (Fig. 1i), as reported in rodents[19]. However, the possibility of direct RGC activation cannot be completely excluded because the stimulation artifact could dissimulate rapid spike initiation.

Vision requires pattern recognition with high spatial resolution, so our next goal was to characterize the response to single electrode activations (Fig. 2a). We wanted to investigate any possible overlap between the current densities produced by two neighboring electrodes which might thus activate the same RGC. RGC activation was obtained at higher stimulation intensities (>4 mW mm^{-2}) and longer stimulation durations (>4 ms), parameters which remain below the radiation safety limits for chronic use[20], (3 retinas, 236 cells, Fig. 2b,c). To further assess spatial resolution of the retinal stimulation by the implant, we mapped the electrical receptive fields (eRFs) of RGCs using single electrode stimulations (4 ms, 10 Hz, 5 mW mm^{-2}) in a pseudo-random manner. Figures 2d-f illustrate the recorded eRF of an RGC responding to a unique pixel #60 (100 µm pitch). When its neighbors were stimulated, it generated no response (Fig. 2f). After sorting the spikes (see methods), 9 of 22 recorded cells responded to only a single electrode (41%), two cells responded to two electrodes when stimulated independently (9%), and the remainder did not respond to any implant stimulation (n=11, 50%). Using a larger pixel size (140 µm), we recorded 77 different single cells from three retinas, with similar results: 41 cells responded to a single electrode (53%) and eight cells to two different electrodes (10 %). The remaining 28 cells (47%) did not respond to any implant stimulation. These results confirmed that, *in vitro*, RGCs can be activated by a single electrode unless they lie at the border of two pixels. To define RGC types activated by these NIR stimulations, we measured their spike propagation velocity as previously described and found that the velocities were consistent with those of midget RGCs[21] (0.56 ± 0.1 m s^{-1}, n=99). Moreover, their single electrode receptive fields were consistent with the small dendritic field of midget cells in the recorded perifoveal area. The absence of parasol cells in the measured cell sample is likely to reflect their lesser density. This selective single electrode activation of midget RGCs provides evidence for high resolution in the blind NHP retina.

We extended the *in vitro* investigation to the human retina (Fig. 3) to assess whether the results we obtained on NHP retina were reproducible with a human retina. A single human eye was dissected 8 hours after the time of death. The tissue state of the postmortem retina did not permit its sectioning, so full-thickness retinal explants were cultured for 48h without any photoreceptor ablation. Apart from some holes in the inner nuclear layer, the tissue structure appeared well preserved (Fig. 3a). Recordings could therefore be obtained from the whole retinal tissue including photoreceptors. Only very few RGCs (n=2) could be recorded because most had degenerated during the postmortem ischemic period prior to tissue preparation. Full field stimulations (100 µm implant) induced RGC action potentials as illustrated on the raster plot and post-stimulus time histogram (PSTH, Fig. 3b) which represent 120 stimulations at 1 ms and 5 mW mm^{-2}, with an enlarged view of the action potentials (Inset Fig. 3b). Figures 3c and d show that the RGC responses from the two RGCs that could be recorded were obtained under similar stimulus conditions to those used for the NHP retina, even though the RGCs were less active in the human retinal preparations than those of the non-human primate. These results confirmed that the retinal implants could effectively activate both non-human primate and human retina.

In vivo study of the implant in behaving macaques

We then wished to test whether NIR activation of these devices could influence the visual perception of awake macaques performing a behavioral task. We first developed the surgery to implant these devices in the sub-retinal space on living NHPs (*Macaca fascicularis*), with a view to further translation of these implants to clinical trials. The implant blocks nutrient flow to the retinal area adjacent to the implant, which causes consecutive separation from the underlying retinal pigment epithelium and choroid, and photoreceptor degradation. This photoreceptor degradation was observed on histological examinations (Supplementary Fig. 1) and multifocal electroretinogram recordings (Supplementary Fig. 2) consistent with a previous study performed in rodents[12]. We implanted a device in one eye of each of three non-human primates (P1, P2 and P3). The implant was positioned parafoveally with an electrode pitch of 140 µm for P1 and 100 µm for P2 and P3 (Fig. 4a-c). The disappearance of photoreceptor layers was confirmed with *in vivo* OCT scans (Fig. 4a-c, bottom pictures). Prior to implantation, the animals had been trained daily to perform a saccade detection task, as follows: after maintaining gaze of central fixation on a square spot for 300 ms, a peripheral stimulation was presented within 9 ms of the central target being removed. The animal was immediately rewarded for saccades in the correct peripheral direction of the visual field, which we divided in 180 angles for mapping visual fields (Fig. 4d). Saccades were considered correct when they reached a window of 5 by 5 degrees centered on the stimulation, between 100 ms and 500 ms after the stimulation

presentation. The animals were initially trained on a standard LCD screen, before being placed before a modified slit-lamp allowing visible and NIR pattern stimulations using a digital micro-mirror device (DMD) (Supplementary Fig. 3). At the end of the training period, the animals were able to perform successful saccades at a rate higher than 90% following visual stimulations. Two other controls were performed ('Control' trials with NIR stimulation outside the implant and 'Catch' trials with no peripheral stimulation). The effectiveness of the implant could therefore be assessed by comparing the simultaneous high success rate following NIR stimulation and the low error rate in control and catch trials.

The local degeneration of photoreceptors adjacent to the implant caused a localized blind spot with photoreceptor degeneration analogous to that of retinal disease. We mapped the entire visual field of each animal by getting the animal to perform some visually guided saccades towards multiple locations (Fig. 4d). Figure 4d illustrates the onset latencies of a correct saccade toward each location, coded by color. This method enabled us to precisely define the locations of the blind spots produced at the implant position for each non-human primate. As illustrated in Figure 4d, the blind spot created by the implant ranged from 9 to 18° for P1 in the lower part of the visual field centered on the coordinates (0; -12). P2's blind spot center was located at (-10; +7.5) subtending 5 to 14°. P2 had some difficulty with performing saccades toward the lower part of the visual field. P3's blind spot was centered on (-8;7.5) in the upper left part of the visual field. We next wanted to test whether any NIR stimulations applied to locations out of the implant induced any saccade. By modulating NIR intensities, we were able to show that the animals were sensitive to NIR stimulations at 600 µW mm^{-2} or above. However, when red light was introduced in the background, the NIR sensitivity threshold increased to 800 µW mm^{-2} (Fig. 4e). All subsequent behavioral tests therefore used stimulations of intensity 800 µW mm^{-2} or below, in the presence of red background light.

The local blind spot created by the implant enabled us to assess whether NIR activation of the implant would activate the corresponding blind retinal area *in vivo*. NIR stimulations were targeted either on the implant, or elsewhere than the implant, as a control. The optical constraints of experimental eye tracking required that the left eye always be recorded, while stimulation was applied to the implanted right eye. This sophisticated saccade detection and stimulation setup was developed as a proxy for the NIR projecting glasses envisioned for human use, which would be impractical in NHP studies. Once the visual fields of the different NHPs had been established, the implants' efficacy could be assessed. The visual field was divided in 36 angles. Blocks of trials were performed. In a typical experimental day, the animal was submitted to 100 to 200 stimulations whose angles were distributed in pseudo-random order. Control and catch trials were added in each block. The high rate of correct trials under visible light enabled us to interleave occasional (<10%) stimulation trials of NIR light pulses (880 nm) without generating animal frustration (Fig. 5a,b). NIR stimulations consisted of six consecutive flashes of 300 µm in diameter, lasting 10 ms every 40 ms. They were generated in three locations over the implant, separated by 5° of visual angle (Fig. 5b). To access animals' perception of a visual percept, animals were rewarded either when making an eye movement toward the stimulated location or when maintaining central fixation for at least 300 ms.

Both animals P2 and P3 responded to NIR stimulations in the direction of the implant with repeated successful saccades. We did not notice such behavioral responses for animal P1 (more details later). Figure 5b shows that, during a block of trials, both animals made saccades toward the target when NIR stimulations were directed toward the implant. To confirm that the NIR stimulations induce a behavioral response only when the stimulation was concomitant with the location of the implant, we added a first type of control trial in which NIR control stimulations were located away from the implant ("NIR control"). Such NIR stimulations away from the implant induced no saccade (Fig. 5b, open red symbols). We also designed two other types of control trials, called catch trials, to confirm that NIR stimulations induce eye movements toward the implant (Fig. 5c). For the first type of catch trial (catch I), the DMD was set to OFF position and the light source was ON and for the second type of catch trials (catch II), the DMD was ON and the light source was OFF. These two additional control conditions allowed us to exclude any peripheral light source as a potential generator of phosphenes. In all three types of control trials (NIR control, catch I and catch II), the animals were rewarded by keeping their gaze within a central window after disappearance of the central spot, but also if the animals made some eye movements toward the potential target. As we noticed with the NIR control trials (Fig. 5b), the animals almost always maintained central fixation during both catch trials (catch I and II, Fig. 5c), rather than making random saccades toward the implant location to be rewarded. The ratio of saccades for control

trials were insignificant for both animals (1.7 %, n=6/345 for animal P2, of which four were eye blinks and 1.9 %, n=4/211 for animal P3). These very few number of evoked saccades during the control trials had neither the latency, nor the spatial accuracy towards the peripheral control position set on the DMD. We are therefore reasonably confident that NIR stimulations away from the implant location did not induce any saccades, and that the DMD or visible light sources were not causally linked to the production of eye movements by producing a peripheral phosphene.

We next characterized the optimal parameters for NIR stimulations for both animals by varying several parameters: NIR intensity, stimulus duration, spot size and number of stimulations (Fig. 6). For animal P2 (Fig. 6a), modulating NIR intensities indicated that the maximum responses to implant stimulation were reached at 300-400 $\mu W\ mm^{-2}$ with a threshold at 200 $\mu W\ mm^{-2}$ (spot size 300 μm). The NIR sensitivity of the implant *in vivo* was therefore well below radiation safety limits for chronic use[20]. It is also below thresholds measured *in vitro*, which could be attributed to a closer interaction with the retinal tissue. At the maximum response, the saccade reproducibility and response latencies (see Supplementary Fig. 4) were comparable to those of natural visible light perception (Fig. 6a). We then modified the other parameters of the NIR spot stimulation: size, number of flashes and flash duration. Decreasing the spot size showed that the response maximum and smallest latencies were attained for a 175 μm spot size on the implant with P2 (Fig. 6a, bottom row). This spot size corresponds to the spot required to fully cover the two photodiodes associated with one electrode (100 μm diameter) regardless of the respective implant position at the back of the eye. Partial activation of neighboring units could also contribute to the visual perception. Visual perception of a single electrode activation is well in agreement with the RGC responses *in vitro* to a single electrode activation (Fig. 2). The recordings obtained from midget cells during single pixel activation *in vitro* are consistent with this *in vivo* observation: firstly, because saccades to static objects have been reported to be possible following midget cell activation[22], and secondly because of the absence of parasol cells in our *in vitro* recording might only reflect their low density in the central retina relative to midget cells. Three flashes, each of 10 ms duration, were sufficient to generate systematic perceptions, whereas the reproducibility of the responses decreased with stimulations shorter than 4 ms (Fig. 6a). These findings agree with our *in vitro* measurements during single electrode activation. For all parameters, the response latencies were gradually reaching similar levels as for saccades in visible light (Supplementary Fig. 4). Two years after implantation, these implant-induced responses were still present without observable change in implant function. These graphs also testify to the ratio of false alarms (evoked saccades during control trials) when NIR stimulations were made away from the implant location to show that NIR stimulations were selective to particular locations.

The stimulation protocol was adapted further for the non-human primate P3 because we did not detect any NIR saccade with the initial settings. The number of NIR stimulations was increased and no reward was delivered if a saccade was not correctly performed following NIR stimulation of the implant or for maintained fixation on the central target. Under these new experimental conditions, we observed that P3 also began to make consistent saccades in response to NIR stimulations only at the implant position (Fig. 6b). No saccade was elicited for certain directions of sight, which decreased the maximum response probability. These gaze directions were thus excluded from the analysis (Fig. 6b). Furthermore, NIR-elicited saccades were obtained only after a period of adaptation to the test procedure (Fig. 6g). NIR responses were elicited at the implant with spot sizes as small as 250 μm (Fig. 6h) and light intensities as low as 200 $\mu W\ mm^{-2}$ (Fig. 6b). The lack of responses in certain directions was attributed to the presence of large clumps of retinal pigment epithelium obstructing visual perception of the implant (Fig. 4c). These results could indicate that the lack of transparency in the retinal tissue may greatly affect the responsiveness of the implant.

While the behavioral results described above were observed in two animals (P2 and P3), no reliable behavioral responses were observed in P1. We had previously shown in the *in vitro* preparations that NIR activation of the implants were responsible for clear artifacts on the MEA recordings (Fig. 1,2). We therefore used *in vivo* electroretinogram recordings to assess the implant functionality for P1, when it failed to show any behavioral responses to NIR stimulations (Fig. 7). We were not able to measure artifacts upon NIR stimulations (up to 5 $mW\ mm^{-2}$) in P1, suggesting that it was not possible to activate its implant (140 μm

pitch) *in vivo* (Fig. 7a). By contrast, in P2 and P3, we measured clear artifacts upon NIR stimulations (Fig. 7a, red traces) using the same equipment as for measuring electroretinograms upon visible light stimulation (Fig. 7a, orange line) with the artifact sizes proportional to the intensity of NIR stimulation (Fig 7b). To verify the functionality of the implant implanted in P1, we sacrificed the animal three years after implantation, extracted the retina, and tested the implant *ex vivo* (Fig. 7c). When we compared the artifacts pre-implantation and post-explantation, we did not observe any change. The implant showed no noticeable physical degradation which suggests that, with the 140 µm electrode pitch; we were not able to properly stimulate P1's implant *in vivo*.

These behavioral results indicate that the photovoltaic sub-retinal implant can stimulate the NHP degenerated retina to elicit a reliable behavioral motor response indicative of phosphene perception.

The promise of human clinical applications

These experiments demonstrated that the NIR-sensitive, fully wireless photovoltaic high resolution implant can activate the blind NHP retina with a single 100 µm electrode resolution *in vitro* and stimulations of 200-250 µm *in vivo* at intensities within radiation safety limits. The high resolution relies on the ground grid configuration confining electrical stimulations, which could have major implications for the development of other brain/machine interfaces. Implantation of the Prima wireless design requires only short, minimally invasive surgery, and enables the use of the natural gaze. Furthermore, the implant lifetime *in vivo* was shown to be at least two years in animals P2 and P3, and three years in P1. The stability of perception and problem-free follow up examinations demonstrate that the retina tolerates the presence of the implant and the electrical stimulation well for prolonged periods. Although the proxy behavioral NHP model and associated experimental saccadic tracking and stimulation setup and adjustment constraints necessarily justify a certain caution in the interpretation of the study, our positive results with the technique were among the elements that led the French and American regulatory agencies to approve it for human clinical trials in dry age-related macular degeneration. This therapeutic strategy could provide a treatment option for geographic atrophy, the advanced form of age-related dry macular degeneration.

Materials and Methods:

Animal models.

The non-human primates in this study were *Macaca fascicularis* of Mauritian origin. Experiments were performed at the Institut du Cerveau et de la Moelle Epiniere (ICM, Paris) and the Molecular Imaging Research Center (MIRCen, CEA, Fontenay aux Roses). All experiments received ethical approval by the French "Ministère de l'Education, de l'Enseignement Supérieur et de la Recherche" under the project references APAFIS#6795-201609201505827 v2 and APAFIS#5929.

Animal behavior methods.

Three male non-human primates (NHP, *Macaca fascicularis*) were used in this study (7-8 years old, 6.5-7.5 kg). They were chair-trained and familiarized with the laboratory and trainers prior to studies. A titanium head post was surgically implanted on top of the NHP skulls with titanium screws. This implantation was realized in sterile conditions. Retinal implant surgery was performed under general anesthesia. After a complete 23-gauge vitrectomy, a retinal bleb was created via sub-retinal injection of balanced salt solution (BSS) around 4 mm away from the fovea. An endodiathermy of 3 mm close to or between the upper retina vessels was performed prior to 2.5 mm retinotomy so that the delivery system with the implant could be presented perpendicular to the retinotomy. This implant insertion instrument was inserted into a 2 mm sclerotomy, 3 mm from the limbus, in order to insert the implant sub-retinally. Perfluorocarbon liquid (PFC) was injected to flatten the detached retinal tissue and stabilize the implant under the retina. Laser coagulation was

performed at the border of the retinotomy (OPHTHALAS 532 EYELITE, Alcon, VITRA-LASER 532 nm GREEN, Quantel Medical). PFC was then removed within a fluid-air exchange. Finally, silicone oil was injected in the eye to ensure retinal reattachment. Silicone oil is known to alter the eye refractivity[23].

Retinal imaging.

Optical coherence tomography (OCT), infrared, and blue reflectance imaging were performed using SPECTRALIS (HRA+OCT, Heidelberg Engineering, Heidelberg). Fundus color photographs were captured with the Smartscope camera (Optomed, Oy, Oulu, Finland).

Multifocal ERG.

Multifocal electroretinography (mfERG) was performed using the RETImap system coupled with the scanning laser ophthalmoscope (SLO) using a binary m-sequence technique (Roland Consult, Germany). The test pattern was in a 30 degree diameter field for 37 hexagons without distortion. Recording was performed at a 59.8 Hz frame rate with 1 kHz (983.5 µs) sampling rate.

Stimulation system.

Our stimulation system, derived from[12], included a single-mode NIR laser (880 nm, 2.5 W, Laser 2000) and a visible light source (590 nm), whose beams were merged together using a dichroic mirror then projected onto a digital micro-mirror device (DMD, DLi innovations, see Supplementary Fig. 3) to generate visual patterns. We mounted the optical system on a slit lamp (Zeiss SL-130). Three NIR non-reflective lenses were placed after the DMD to create a collimated image of the DMD pattern.

Behavior.

- *Saccade detection task*

The animals were trained daily to perform a saccade detection task and were rewarded for making saccadic eye movements from a central square fixation point to a peripheral circular spot. Once central fixation was achieved for 300 ms on a square spot (300 µm), a peripheral stimulation was presented within less than 9 ms while removing the central target. The default peripheral stimulations consisted of a 300 µm diameter circle presented for 210 ms. The entire visual field was divided in 36 to 180 angles all separated by 10° to 2° respectively angles on a circle of known eccentricity. The stimulations in each trial were presented in a pseudo-random order. Due to the optical constraints, the left eye was used for eye-tracking as the implanted right eye was stimulated. Daily training involved immediate rewards for proper center-out saccades in the correct peripheral direction in the visual field. Up to 10 trials were recorded daily. Saccades were considered correct when the animal gaze reached a 5 by 5° window surrounding the target.

- *Visual field mapping*

For the visual field mapping, 180 stimulations of 2° of stimulation were presented for each eccentricity. No controls were added to these trials as these experiments' only purpose was to locate blind spots.

- *NIR implant stimulations*

The high rate of correct trials under visible light enabled us to interleave occasional (<10%) stimulation trials of NIR light pulses (880 nm) without generating animal frustration. NIR stimulations consisted in 6 consecutive flashes of 300 µm in diameter (or less for trials studying NIR stimulation size), lasting 10 ms every 40 ms. The total duration between the onset of the first stimulation and end of the last stimulation was

210 ms. Three locations over the implant, separated by 5° of visual angle, were included in each trial. These trials were repeated over three different eccentricities.

- *Control trials*

We designed three different types of control trials to confirm that NIR stimulation were selective to the implant location: (1) The first control trial, NIR control trial, consisted of stimulating healthy parts of the visual field (away from the implant locations) with NIR stimulations. These NIR control trials were important to insure that saccades induced by NIR stimulations were only due to the implant stimulations and not to natural vision. (2) The first type of catch trial (catch I), the DMD was set to the complete OFF position and the light source was set ON. (3) In the second type of catch trial (catch II), the DMD was set ON although the light source was set OFF. The catch trials (I and II) allowed us to check whether any reflected light generated by the DMD or the light source might be responsible for inducing eye movements. For these three different types of control trials (NIR control, catch I and catch II), the animals were both rewarded for maintaining fixation for 300 ms or making an eye movement toward the potential target. These trials ensured that the animals did not have any tendency to realize saccades toward the implant location by guessing. For Figure 6, we categorized a trial as a *false alarm* when the animal made some saccade during NIR control trials.

To calculate the distance for the peripheral target presentation, we used the reported correspondence of 200 µm deg^{-1} in non-human primates[24].

- *Changes in proportion of trials for P3*

When P3's implant was stimulated using NIR, the animal mainly fixated to get its reward. We hypothesized that the primate preferred to get a reward from fixating rather than doing a saccade towards a phosphene that could potentially be blurry. We therefore increased the number of NIR stimulations on the implant and we did not deliver a reward upon fixation following a NIR stimulation of the implant.

Implant characterization.

The implant electrical output characterization is performed by stimulating single pixels with controlled 880 nm laser irradiance pulsed at 4 ms pulse duration, 30 Hz frequency, immersed in a saline solution with 1400 µS/cm conductivity, and recording with a neural type micro-electrode (Alpha Omega Co., USA) whose tip was positioned 20 µm above the implant pixel electrode and connected to a differential amplifier (AM-system LLC, USA). This setup typically has a relatively high measurement variability of approximately +/- 30% due to the number and complexity of variable parameters that must be controlled during measurement, such as solution conductivity, laser irradiance stability, temperature, micrometer level electrode positioning, and recording electrode impedance states. The two measurement curves of Fig. 7c are therefore considered to be equivalent and their amplitude difference can be attributed to the imprecision of the characterization setup.

Sacrifice and harvest of retinal tissues.

NHPs received a lethal dose of pentobarbital. Eyeballs were removed and placed in sealed containers for transport with CO_2 independent medium (ThermoFisher scientific), after transcorneal puncture of the eye with a sterile 20-gauge needle. Retinas were then isolated and dissected either for histology or for retinal explant culture.

Retinal explant culture.

Retinal tissues were preserved in CO_2 independent medium (ThermoFisher scientific). To produce a blind NHP retinal model, the retina was transversely sectioned to remove the photoreceptor layer as previously reported for transplantation of photoreceptor layers[25]. A square piece of retinal tissue (2x2 mm²) was cut at its four corners to flatten it photoreceptor-side down on a flat pork skin based gel block. A razor blade cut 100-110 µm deep from the vitreal surface was performed to isolate the inner retina. These inner retinal tissues were maintained in culture for 12 to 36 hours on polycarbonate transwell (Corning) in Neurobasal + B27 medium.

Multi electrode array recordings.

Retinal explants were transferred onto a cellulose membrane preincubated with polylysine (0.1%, Sigma) overnight. A NIR-sensitive photovoltaic implant was inserted on the cellulose membrane with implant electrodes facing the photoreceptor side of the retinal explant. Using a micromanipulator, the retinal explant was gently pressed against a multi-electrode array (MEA256 100/30 iR-ITO; Multi-Channel Systems, Reutlingen, Germany), with the retinal ganglion cells facing the MEA recording electrodes. The retinal tissue was continuously perfused with Ames medium (Sigma-Aldrich, St Louis, MO) bubbled with 95% O_2 and 5% CO_2 at 35 °C at a rate of 8 mL min^{-1}. Spontaneous spiking activities from retinal ganglion cells (RGCs) were recorded after high-pass filtering the signals from each electrode (Butterworth filter, second order, cut-off frequency 300 Hz). Spikes were attributed to individual cells using an in-house spike-sorting algorithm. Spike velocity were then calculated according to a previously reported protocol[18]. The implant was stimulated through the MEA using an NIR laser (2.5 W, 880 nm Laser 2000). This laser was identical to those used by Pixium Vision during electro-optical characterizations. Output light intensities were calibrated to range from 0.1 mW mm^{-2} to 5 mW mm^{-2} while NIR patterns were created using the DMD (DLi innovations). To distinguish whether the NIR-elicited spikes originated from bipolar cells or direct RGC activation, the glutamate receptor blockers, LAP-4 (50 µM) and CNQX (100 µM) were added to the AMES medium. RGC activity was defined as the average number of action potentials in a 40-ms window starting after the end of the stimulation artifact. This instant varied with the stimulation artifact. The latter lasted during the stimulation pulse and prevented spike detection within that period. The cell response threshold was set at level that exceeded cell spontaneous activity three-fold.

Histology.

Retinal tissues were fixed overnight in 4% (wt/vol) paraformaldehyde in phosphate buffered saline (PBS; 0.01M, pH 7.4) at 4°C. The tissue was cryoprotected in successive solutions of PBS containing 10%, 20% and 30% sucrose at 4 °C and embedded in OCT (Labonord, Villeneuve d'Ascq, France). Retinal sections were permeabilised for five minutes in PBS containing 0.1% Triton X-100 (Sigma, St. Louis, MO) and rinsed. For immunolabelling, retinal fragments were incubated in a blocking solution in PBS (1% bovine serum albumin (Eurobio, Les-Ulis, France), 0.1% Tween 20 (Sigma)) for 1 h at room temperature. They were then incubated for one night at 4°C with primary antibodies in a blocking solution. The antibodies used were a monoclonal antibody directed against mouse G0α (1:200, Chemicon, Darmstadt, Germany) and a polyclonal rabbit cone arrestin (Luminaire junior, LUMIj, 1:20,000, a gift from Prof. Cheryl Craft). The fragments were rinsed and then incubated with secondary antibodies: donkey anti-mouse IgG and donkey anti-rabbit IgG antibodies conjugated to Alexa™488 and Alexa™594, respectively (1:500, Molecular Probes, Invitrogen, Eugene, Oregon) for 1 h at room temperature. Cell nuclei were stained with 4′,6-diamidino-2-phenylindole (DAPI), which was added during the final incubation period. Sections were rinsed then mounted with Fluorsave reagent (Permafluor) on a microscope slide. Confocal microscopy was performed on an Olympus FV1000 laser-scanning confocal microscope.

Data availability statement

The authors declare that all data supporting the results in this study are available within the paper and its Supplementary Information. The raw and analysed datasets generated during the study are available for research purposes from the corresponding authors on reasonable request.

Code availability statement

The code that supports the findings of this study are available from the corresponding author upon reasonable request.

References

1. Brandli, A., Luu, C. D., Guymer, R. H. & Ayton, L. N. Progress in the clinical development and utilization of vision prostheses: an update. *Eye Brain* **8**, 15 (2016).
2. Cha, K., Horch, K. & Normann, R. A. Simulation of a phosphene-based visual field: visual acuity in a pixelized vision system. *Ann. Biomed. Eng.* **20**, 439–449 (1992).
3. Cha, K., Horch, K. W., Normann, R. A. & Boman, D. K. Reading speed with a pixelized vision system. *JOSA A* **9**, 673–677 (1992).
4. Fornos, A. P., Sommerhalder, J., Pittard, A., Safran, A. B. & Pelizzone, M. Simulation of artificial vision: IV. Visual information required to achieve simple pointing and manipulation tasks. *Vision Res.* **48**, 1705–1718 (2008).
5. Sommerhalder, J. *et al.* Simulation of artificial vision: I. Eccentric reading of isolated words, and perceptual learning. *Vision Res.* **43**, 269–283 (2003).
6. Sommerhalder, J. *et al.* Simulation of artificial vision: II. Eccentric reading of full-page text and the learning of this task. *Vision Res.* **44**, 1693–1706 (2004).
7. Jung, J.-H., Aloni, D., Yitzhaky, Y. & Peli, E. Active confocal imaging for visual prostheses. *Vision Res.* **111**, 182–196 (2015).
8. Stingl, K. *et al.* Interim results of a multicenter trial with the new electronic subretinal implant Alpha AMS in 15 patients blind from inherited retinal degenerations. *Front. Neurosci.* **11**, 445 (2017).
9. Da Cruz, L. *et al.* The Argus II epiretinal prosthesis system allows letter and word reading and long-term function in patients with profound vision loss. *Br. J. Ophthalmol.* **97**, 632–636 (2013).
10. Joucla, S. & Yvert, B. Improved focalization of electrical microstimulation using microelectrode arrays: a modeling study. *PloS One* **4**, e4828 (2009).
11. Bendali, A. *et al.* Synthetic 3D diamond-based electrodes for flexible retinal neuroprostheses: Model, production and in vivo biocompatibility. *Biomaterials* **67**, 73–83 (2015).
12. Lorach, H. *et al.* Photovoltaic restoration of sight with high visual acuity. *Nat. Med.* **21**, 476 (2015).

13. Picaud, S. *et al.* GABAA and GABAC receptors in adult porcine cones: evidence from a photoreceptor-glia co-culture model. *J. Physiol.* **513**, 33–42 (1998).

14. Jones, B. W. *et al.* Retinal remodeling and metabolic alterations in human AMD. *Front. Cell. Neurosci.* **10**, 103 (2016).

15. Jensen, R. J., Ziv, O. R. & Rizzo, J. F. Thresholds for activation of rabbit retinal ganglion cells with relatively large, extracellular microelectrodes. *Invest. Ophthalmol. Vis. Sci.* **46**, 1486–1496 (2005).

16. Fried, S. I., Hsueh, H.-A. & Werblin, F. S. A method for generating precise temporal patterns of retinal spiking using prosthetic stimulation. *J. Neurophysiol.* **95**, 970–978 (2006).

17. Freeman, D. K., Rizzo III, J. F. & Fried, S. I. Encoding visual information in retinal ganglion cells with prosthetic stimulation. *J. Neural Eng.* **8**, 035005 (2011).

18. Boinagrov, D., Pangratz-Fuehrer, S., Goetz, G. & Palanker, D. Selectivity of direct and network-mediated stimulation of the retinal ganglion cells with epi-, sub-and intraretinal electrodes. *J. Neural Eng.* **11**, 026008 (2014).

19. Mathieson, K. *et al.* Photovoltaic retinal prosthesis with high pixel density. *Nat. Photonics* **6**, 391 (2012).

20. Lorach, H. *et al.* Retinal safety of near infrared radiation in photovoltaic restoration of sight. *Biomed. Opt. Express* **7**, 13–21 (2016).

21. Li, P. H. *et al.* Anatomical identification of extracellularly recorded cells in large-scale multielectrode recordings. *J. Neurosci.* **35**, 4663–4675 (2015).

22. Schiller, P. H. & Lee, K. The effects of lateral geniculate nucleus, area V4, and middle temporal (MT) lesions on visually guided eye movements. *Vis. Neurosci.* **11**, 229–241 (1994).

23. Smith, R., Smith, G. & Wong, D. Refractive changes in silicone filled eyes. *Eye* **4**, 230 (1990).

24. Lapuerta, P. & Schein, S. J. A four-surface schematic eye of macaque monkey obtained by an optical method. *Vision Res.* **35**, 2245–2254 (1995).

25. Silverman, M. & Hughes, S. Transplantation of photoreceptors to light-damaged retina. *Invest. Ophthalmol. Vis. Sci.* **30**, 1684–1690 (1989).

Acknowledgements

Author contributions

P-H.P., P.D., G.C., P.P., R.B., and S.P. planned the studies. M.L., M.V., K.B., and F.A. conducted the NHP behavioral experiments assisted by N.W., and M.W. S.D., V.F. conducted the *in vitro* experiments. E.D., and S.D. performed the histological analyses. K.G., H.A., and M.A.K, analyzed the data. K.B., and O.O., coded the stimulations. P.L., E.E., and H.L, built the apparatus. Y.L., E.Bo., M.D., and R.H., designed the surgery procedure. E.Br., C.N-J., P.H., J.D., C-M.F., and Y.L. realized the prostheses surgeries. E.Bo., M.D., R.H., and G.B characterized and provided the implants. P-H.P, S.P., P.P., F.A. wrote the paper. J-A.S., and S.P. obtained funding. All authors reviewed, edited, and approved the paper.

Competing interests

Additional information

Figures

Figure 1:

Figure 2:

Figure 3:
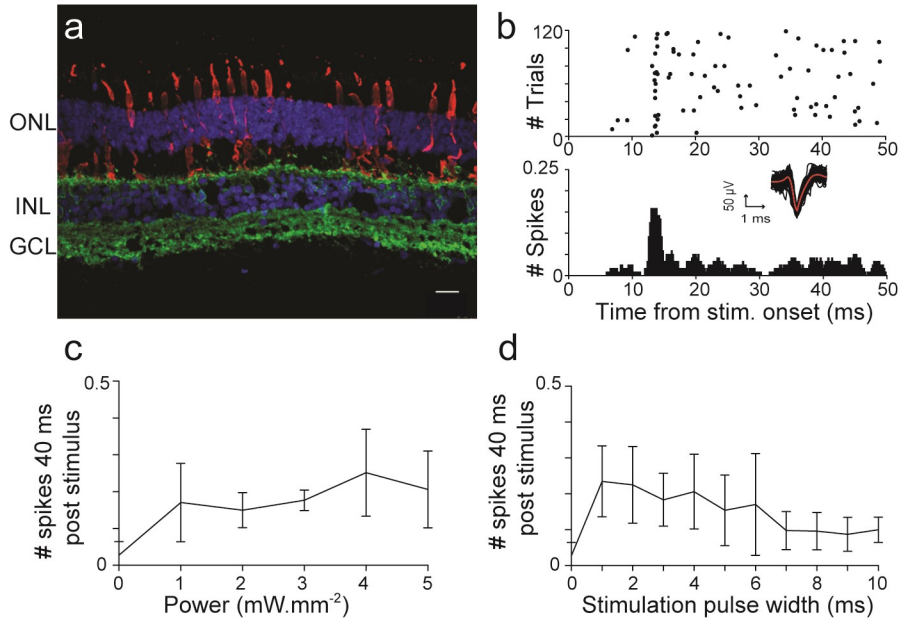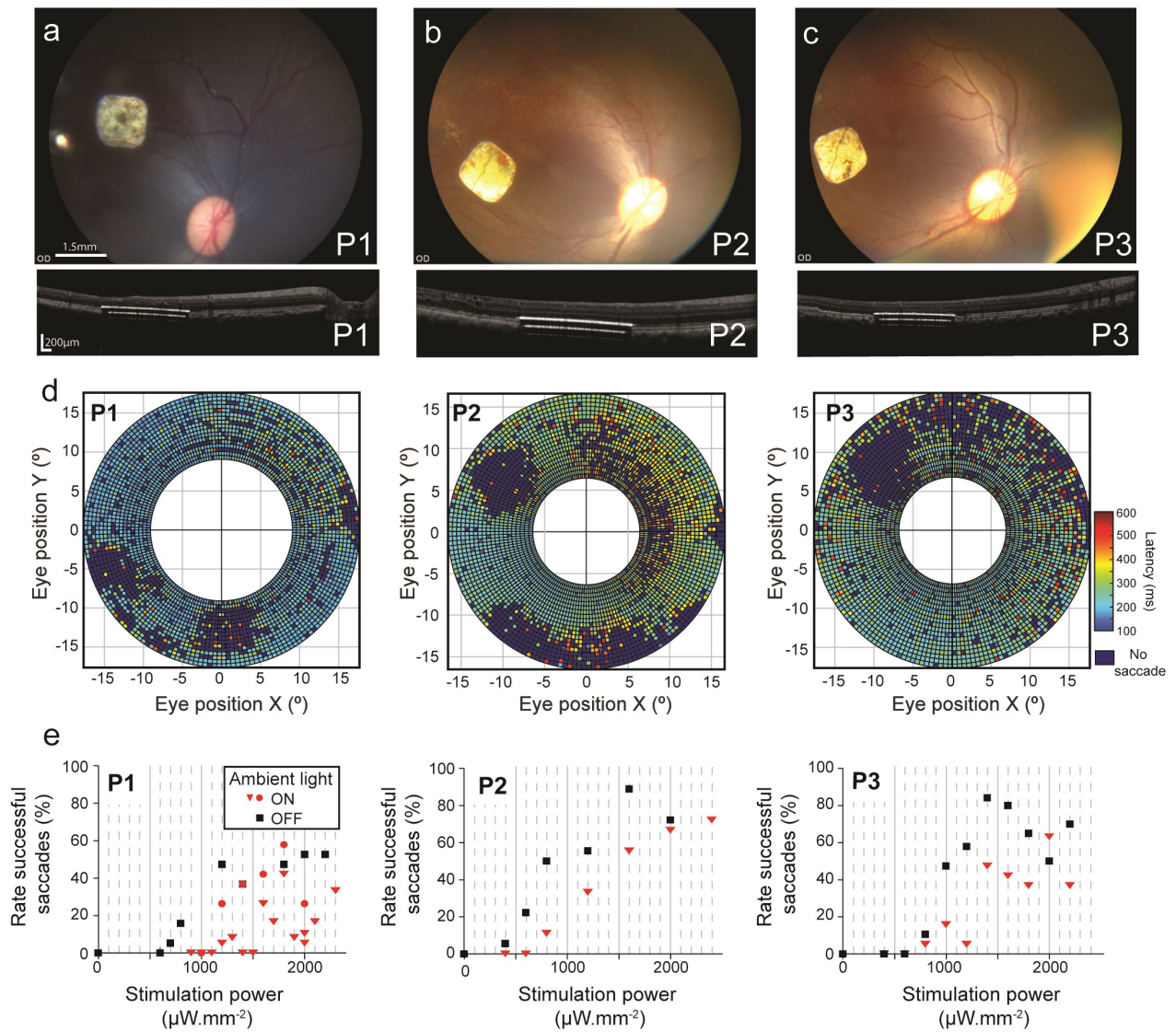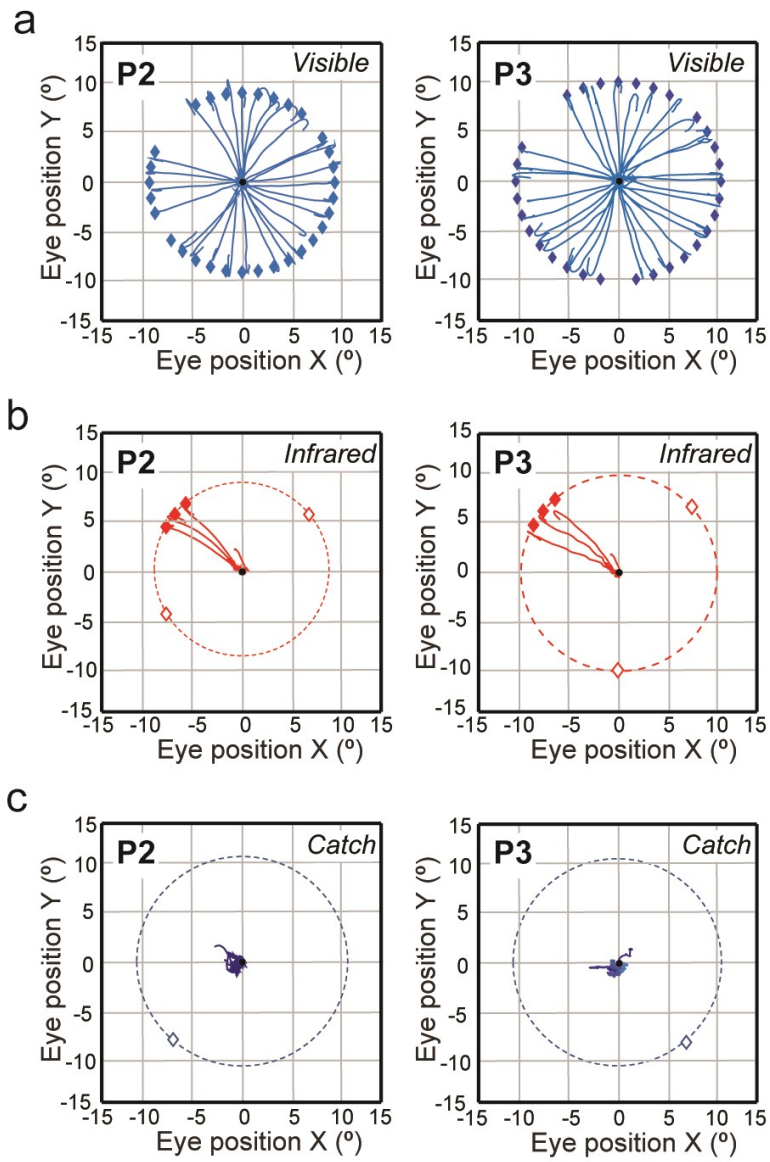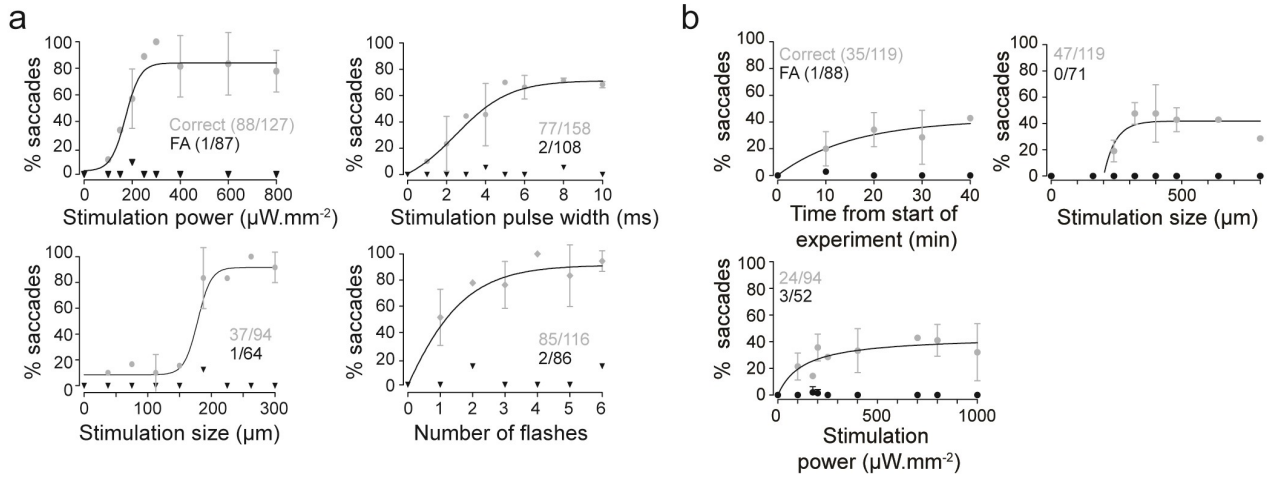
Figure 4:

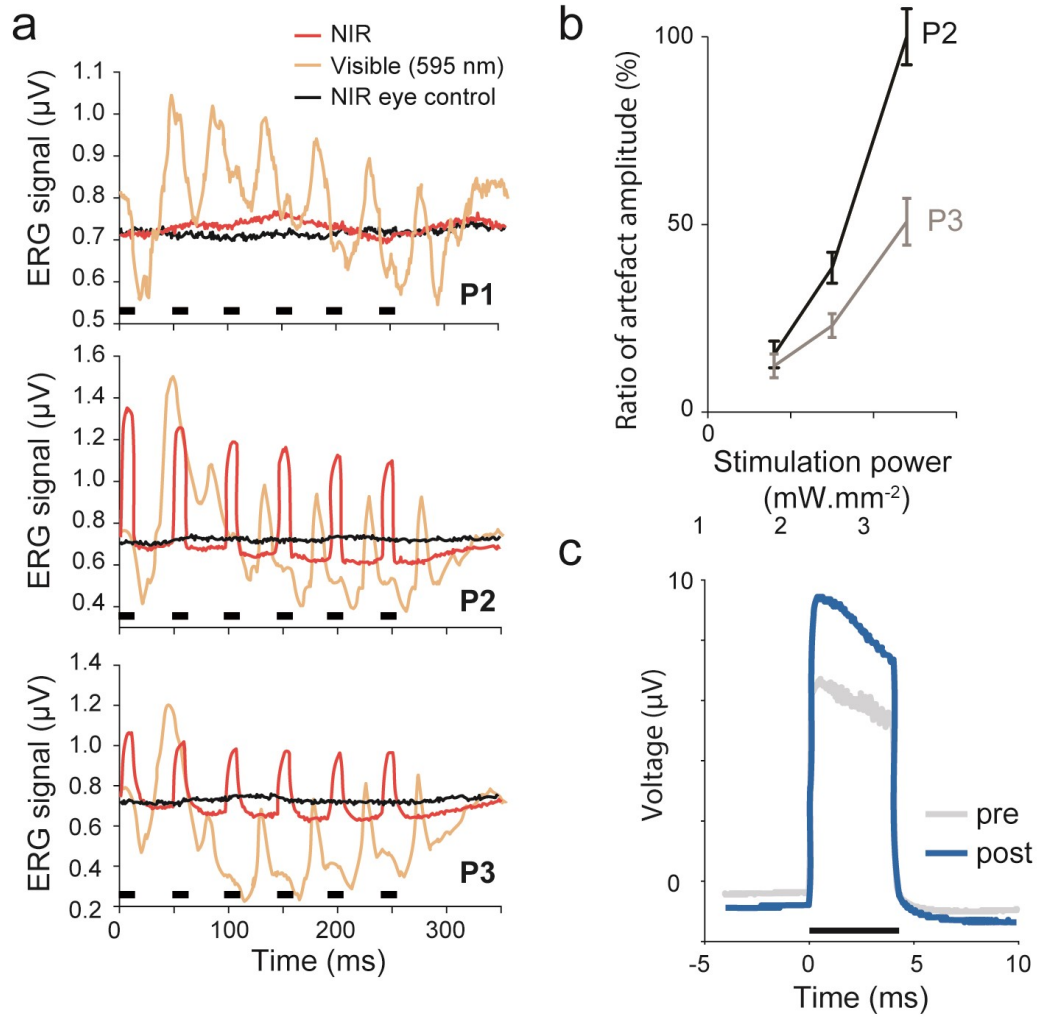**Figure 5:**

Figure 6:

Figure 7:

Figure captions

Fig. 1 | Retinal prosthesis design and retinal ganglion cells responses on an *in vitro* non-human primate (NHP) retina preparation. a, Retinal implant design with 205 electrodes. Each electrode is 140 μm wide. Scale bar: 280 μm. Inset: wiring diagram for a single implant unit, consisting of two photodiodes connected in series between the active central electrode (1) and the surrounding ground grid (2). **b**, Histological section of a control NHP retina. Scale bar: 20 μm (ONL: outer nuclear layer; INL: inner nuclear layer; GCL: ganglion cell layer). Photoreceptors (PR) are labeled by cone arrestin in red and cell nuclei by DAPI (white). **c**, Histological section of NHP retina after vibratome sectioning of the photoreceptor layers. The intact and sectioned tissues in (**b**,**c**) were cultured for a day prior to recording and were fixed after the experiment. **d**, Schematic of the implanted retina during multi-electrode array (MEA, in gray) recording sessions. The implant is in yellow and electrodes are schematized as horizontal blue bars whereas RGCs are indicated as blue circles, bipolar cells in blue diamonds, amacrine cells in orange circles and horizontal cells in brown circles. **e**, Activity recorded at one electrode during a MEA recording session showing RGC spikes generated in response to a full-field stimulation (4 ms and 2 mW mm^{-2}, 100 μm width pixel). Data were high pass-filtered (cut-off frequency of 300 Hz). The gray rectangle represents the 40-ms period after the artifact in which the spikes were counted. **f**, Raster plot gathering action potentials timings after 300 stimulations at 2 Hz. The gray rectangle represents the 40-ms period. **g**, Threshold measurements after full-field stimulations while varying NIR illumination power with 4 ms pulses (2 retinas, 166 cells, 100 μm width pixels). **h**, Threshold measurements after full-field stimulations with varying NIR stimulation pulse widths at 1 mW mm^{-2} (2 retinas, 166 cells, 100 μm width pixels). **i**, Spike counts during application of synaptic blockers (LAP4 CNQX-CPP) showing the suppression of the implant-elicited stimulation. The RGC activity increases during NIR stimulation (stim) from a background level of spontaneous activity (SA), then progressively disappears during the application of blockers to the bath (30 and 50 minutes, pixels 100 μm, 120 stimulations at 2 Hz, 10 ms, 4 mW mm^{-2}). Error bars in **g/h/i** represent the standard deviation (SD), centered on the mean.

Fig. 2 | RGC responses to single pixel activations on an *in vitro* blind NHP retina. a, Photography of the implant (black circle) on the blind NHP retina positioned on a MEA; black dots around the dark shadow of the implant represent the MEA electrodes. A NIR stimulation induces a single pixel activation (top right). Pixel width and scale bar: 140 μm. **b**, Threshold measurement after single electrode stimulations while varying NIR illumination power with 4 ms pulses. **c**, Threshold measurement after single electrode stimulations with varying NIR stimulation pulse widths at 4 mW mm^{-2}. (**b**,**c**) Data from n=236 recorded cells from 3 retina. Error bars represent the standard deviation centered on the mean. **d**, Example of one recording showing a burst of spikes from RGCs following single pixel stimulations of electrode #60. No responses were observed when distant electrodes (#12, #23 and #55) were stimulated (parameters of stimulation: 4 ms and 4 mW mm^{-2}). 9 of 22 recorded cells responded in a similar manner. Gray rectangles schematized the 40-ms period within which the spikes were counted. **e**, Spike histogram of the RGC activity in (**d**) showing an increase in its spiking frequency for pixel 60 only (4 ms and 5 mW mm^{-2}). **f**, Electrical receptive field of the RGC recorded in (**e**) after stimulation of individual implant electrodes (100-μm pitch). Scale bar: 100 μm.

Fig. 3 | In vitro experiment on a human retina after full field stimulation. a, Cross sections of a human retina. Cones were marked using cone arrestin (red), bipolar cells with G0$_\alpha$ (green), and cell nuclei with DAPI (blue). Holes in the retina are shown by the lack of regularity in the cone organization. Scale bar: 20 μm. **b**, Raster plot and post-stimulus time histogram (PSTH) after 120 full-field stimulations at 1 ms and 5 mW mm^{-2}. Full-field measurements were performed using an implant with 100 μm pixels. Inset: waveforms of the recorded action potentials. The red line represents the average waveform. **c-d**, Response rates in a 40-ms window following the stimulus as a function of either NIR power (**c**) or the stimulus durations (**d**). Data from n=2 recorded cells from 1 retina. Default conditions; 4 ms, 5 mW mm^{-2}. Error bars in **c/d** represent the standard deviation centered on the mean.

Fig. 4 | Ophthalmological characterization and natural vision of implanted non-human primates. a-c, Fundus at two weeks post implantation for P1-3. The implants are all located in the exterior part of the Area Centralis. OCT section at the implant locations in P1-3, implants are subretinal and above the choroid. **d**, Visual fields of P1-3 respectively, after central fixation, a peripheral visible stimulation (half a degree) was

presented every 2° in the periphery. The latencies of the saccades are depicted by color. Each target was presented to the primates only once. The targets that did not induce a successful saccade are presented in dark blue. The different blind spots (large dark blue areas) correspond to the implant, the effects of surgery, and the optic nerve. The implant blind spots are in the lower (P1) and upper left part (P2 and P3) of the visual fields, indicated by a red asterisk. The effects of surgery were present on the lower left part of the visual field of P1. The optic nerve blind spots are all on the right side of the visual field. **e**, NIR natural vision for P1-3 respectively, with and without ambient red light which was aimed at creating a background to reduce natural perception of NIR stimulation. Implants are 1.5 mm in size. Triangles and discs represent two different experimental days.

Fig. 5 | Implant activation in a behaving monkey. Visible and NIR stimulations in behaving NHPs. **a**, These panels represent the correct saccades made by both animals (P2 left quadrant and P3m right one) after visible stimulations during one trial (n=31). After fixating a central spot (black dot) for 300 ms, a peripheral stimulation (2 degrees, blue diamonds) is presented every 10° in the periphery. **b**, With NIR stimulation (red diamonds), the animals generate correct saccades only in the area where the implants were located. For control trials with the stimulation of healthy parts of the retina with NIR stimulations (open red diamonds), the animals made no saccades. NIR stimulations could occur at any location on the red dashed circle. **c**, For catch trials (without any light source ON or DMD off), no saccade was observed in either animal P2 or P3. Open blue diamonds represent the potential location of the target, while the targets could be located anywhere within the eccentricity schematized by the dashed blue circle.

Fig. 6 | Optimal parameters for NIR stimulations. a, Percentages and successful saccades (gray symbols) towards the implant when varying either the NIR power, stimulation spot size, pulse width or number of flashes (by default spot size: 300 μm, illumination power: 800 μW mm^{-2}, stimulation pulse width: 10 ms, number of flashes: 6). Black symbols represent the ratio of false alarms (FA) for the different parameters of the NIR stimulations. These four panels report the performance of monkey P2 only. Gray: total number of correct saccades and total number of NIR stimulations toward the implant. Black: total number of false alarms and total number of NIR stimulations out from the implant. **b**, Percentages of saccades (gray symbols) towards the implant by duration after the onset of the behavioral test, spot sizes, and NIR power, for monkey P3 only. Default stimulation parameters were spot size 300 μm, power 800 μW mm^{-2}. Black circles: false alarm ratios. Error bars in **a/b** represent the standard deviation centered on the mean.

Fig. 7 | Electro optical characterization of the implant. a, Electroretinograms for P1, P2 and P3 after NIR stimulation (red for NIR in implanted eye and black for NIR in other eye) and visible stimulations (orange). NIR-elicited artifacts on P1, P2, and P3 following either six flashes of visible illumination (595 nm - orange curve) or NIR illumination (2.4 mW mm^{-2}, red curve). Note the absence of artifact in P1 upon NIR stimulations (red trace). Similarly, NIR flashes did not induce any response in the control non-implanted eye (2.4 mW mm^{-2}, black curves) for all three animals. Full field flash durations (infrared and visible) are indicated above the X-axis by black dash lines. **b,** Amplitudes of NIR stimulation artifacts for monkeys P2 and P3 at three different intensities. NIR stimulations for monkey P1 induce no artifact as shown in **a**. **c,** Voltage measurement above a single pixel stimulation at 5 mW mm^{-2} pre-implantation and post-explantation on the prosthesis implanted in P1. Error bars in **b** represent the standard deviation centered on the mean, data from 20 stimulations of 6 flashes.